




Bloch oscillations of backward volume magnetostatic spin wavesA. S. Laurenson , J. Bertolotti , and V. V. Kruglyak **University of Exeter, Stocker Road, Exeter, EX4 4QL, United Kingdom*

(Received 13 August 2019; revised 30 May 2020; accepted 27 July 2020; published 10 August 2020)

We have used numerical micromagnetic simulations to propose a feasible candidate system in which Bloch oscillations of spin waves could be observed experimentally. Our simulations demonstrate these phenomena for backward volume magnetostatic spin waves (BVMSWs) in a film of yttrium-iron-garnet in a spatially varying bias magnetic field comprising a sinusoidal and gradient contributions. Despite the complex character of the BVMSW dispersion relation, the spin-wave packets are distinctly confined by the field gradient, while showing only minor broadening over the simulation time.

DOI: [10.1103/PhysRevB.102.054416](https://doi.org/10.1103/PhysRevB.102.054416)

In 1929, Bloch made a surprising prediction that electrons in a perfect crystal subject to a uniform electric field do not propagate, but instead oscillate back and forth around a mean position, in a phenomenon now known as Bloch oscillations [1]. In the reciprocal space, this corresponds to oscillations of an electron wave packet within an electron band due to reflection from the band gaps at the Brillouin-zone boundaries. However, the period of the oscillations scales inversely with the crystal's lattice constant, making it too long compared to the electron coherence time to be observable even in the most perfect crystals. Only in 1992, when advances in the nanotechnology facilitated fabrication of high-quality semiconductor superlattices, Bloch oscillations of electron wave packets under a bias voltage were detected experimentally [2,3]. At high electric fields, the electrons may also tunnel resonantly between neighboring bands, causing what is known as Landau-Zener tunneling (breakdown) [4]. Such phenomena are not unique to electrons in crystals and superlattices but can occur for any waves in periodic media with a gradient variation of their properties. This gradient plays the same role for the waves as the accelerating electric field plays for electrons. Optical [5–8], acoustic [9–11], and cold atom arrays [12–14] have all been shown to support Bloch oscillations. In systems with a strong spin-orbit coupling, Bloch oscillations of electrons can also be induced by a gradient magnetic field [15,16].

Despite the marked advances in the physics of Bloch oscillations in general, Bloch oscillations of spin waves—wavelike excitations of the magnetization in magnetically ordered materials [17]—have not been observed so far. Periodically modulated magnetic media for spin-wave propagation, known as magnonic crystals [18–20], form an active research area in modern magnonics [21–24]. Strategies for the realization of magnonic crystals include geometric patterning [25,26], compositional modulation [27], modulated applied magnetic field [28], or even heating [29]. In principle, any

such magnonic crystal could either be produced with a gradient of its characteristics, or one could induce the gradient, e.g., by heating [30] or by applying a gradient bias magnetic field [31–34]. However, the authors of Refs. [30–34] have only studied the regime of small gradients, which are insufficient to produce Bloch oscillations. On the theory side, Bloch oscillations were proposed for exchange spin waves, which have a parabolic dispersion relation [35–37]. In this case, the wave equation is very similar to the Schrödinger equation for a quantum-mechanical particle, with the bias magnetic field playing the role of the potential [38]. This approach is convenient theoretically and allows one to reproduce the same physics as for the electron Bloch oscillations. However, this exchange-dominated regime is somewhat remote from the experiment, in which magneto-dipole and dipole exchange spin waves are primarily studied [21,24,26,29–33]

Here, we use micromagnetic simulations [39] to demonstrate feasibility of observation of Bloch oscillations of backward volume magnetostatic spin waves (BVMSWs) in *realistic* magnonic crystals. The latter are formed by applying a bias magnetic field that is spatially nonuniform in the direction of spin-wave propagation in a thin film [Fig. 1(a)] of yttrium-iron-garnet (YIG). The field profile has two contributions: one linear and one sinusoidal [40]. Our simulations demonstrate Bloch oscillations for a realistic set of sample parameters and experimental conditions. Furthermore, they reveal features of these phenomena that are inherent to spin waves but are not usually encountered for waves of other origins.

Let us begin by highlighting general features expected for Bloch oscillations of spin waves. We consider a wave packet with a central frequency ω_0 that propagates in a magnonic crystal under action of a static bias magnetic field $H(x)$ that depends linearly on coordinate x with a gradient $G \equiv \partial H/\partial x$ [41]. The central frequency remains constant, i.e.,

$$\omega_0 = \omega[k(x), H(x)] = \text{const}, \quad (1)$$

where $k(x)$ is the packet's central Bloch wave number. We assume that the latter follows the magnetic-field gradient adiabatically, so as to ensure that the spin-wave dispersion relation $\omega(k, H)$ may still be introduced and is satisfied for

*Corresponding author: V.V.Kruglyak@exeter.ac.uk

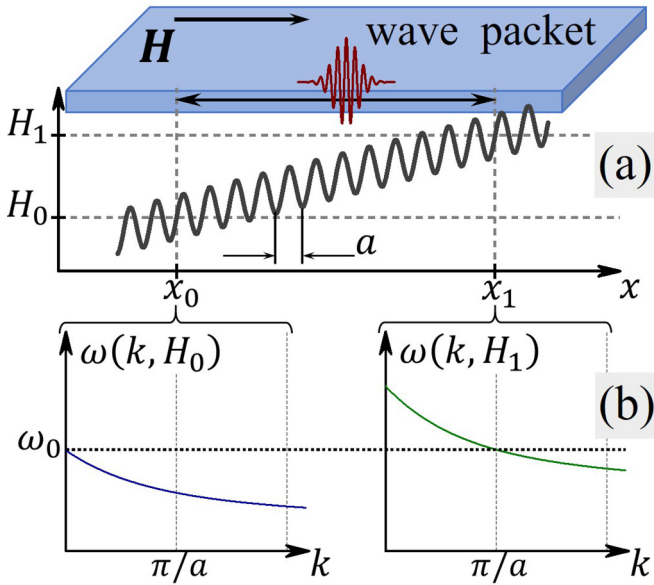


FIG. 1. The geometry of the problem is shown schematically. (a) Nonuniform magnetic field $\mathbf{H}(x)$, combining the gradient and sinusoidal contributions, is applied to a uniform film of YIG along the direction of spin-wave propagation. (b) The field corresponds to the uniform FMR frequency ($k = 0$) in point x_0 (field H_0) and to the first Brillouin-zone boundary ($k = \pi/a$) in point x_1 (field H_1), for which the BVMSW dispersion is schematically shown. The spin-wave wave packet is excited by a uniform microwave magnetic field in point x_0 and then bounces back and forth periodically between points x_0 and x_1 , thereby being confined to a region of size $L = x_1 - x_0$.

each value of x . Differentiating Eq. (1), we obtain

$$\left(\frac{\partial \omega}{\partial k}\right)_H dk + \left(\frac{\partial \omega}{\partial H}\right)_k dH = 0, \quad (2)$$

where the first and second terms may be interpreted as changes in the kinetic and potential energy of the wave packet, respectively. To conserve the frequency, the two changes must be equal and opposite. Furthermore, we can write Eq. (2) as

$$\frac{dk}{dt} = -G \left(\frac{\partial \omega}{\partial H}\right)_k \equiv F, \quad (3)$$

which can be identified as the equation of motion of the wave packet under action of the “effective force” F due to the nonuniform magnetic field [11,42,43].

The Bloch oscillations occur due to the wave packet making round trips within the Brillouin zone after being backscattered from the points (both in the real and reciprocal spaces) at which the frequency acquires its maximum and minimum values for a particular band. For our case of BVMSWs, this occurs when the wave number acquires values of 0 and π/a , respectively, where a is the lattice constant of the magnonic crystal. So, the period of Bloch oscillations T_B is obtained by integrating the equation of motion (3) as

$$T_B = - \int \frac{dk}{F}, \quad (4)$$

where the integration is performed over one Brillouin zone.

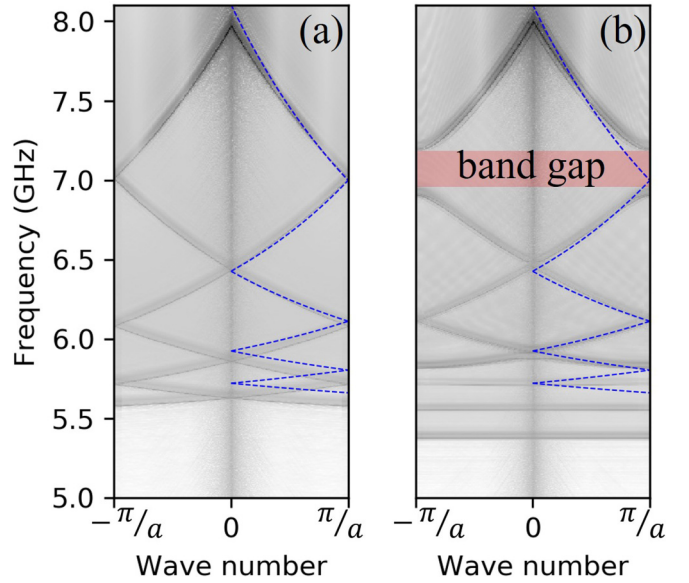


FIG. 2. The magnonic dispersion relations are shown in the reduced zone scheme for (a) the uniform and (b) periodically modulated 1- μm -thick films of YIG for a uniform bias magnetic field of 185 mT. The grayscale shows the results of the numerical simulations (darker color corresponds to higher Fourier amplitude of spin waves), while the dashed line shows the analytical dispersion calculated using Eq. (6) and folded into the first Brillouin zone.

When F does not depend on x , it must also be independent of k , due to Eq. (1). Then, the wave number is expected to depend linearly on time, while Eq. (4) reduces to the conventional form

$$T_B = 2\pi/aF \text{ or } \omega_B = aF, \quad (5)$$

where ω_B is the angular frequency of the Bloch oscillations. For instance, for exchange spin waves considered in Refs. [35–37], $F = -\mu_0\gamma G$, where μ_0 is the permeability of free space, γ is the gyromagnetic ratio, while $G < 0$ for waves with a positive group velocity. Similarly, for a quantum-mechanical particle, we can associate H with the potential energy, and then $F = -\hbar^{-1}G$, where \hbar is the Planck constant and $-G$ is the usual mechanical force.

In the general case of magneto-dipole (e.g. BVMSWs) and dipole-exchange spin waves, F is a function of k . Indeed, we may approximately consider the dispersion of BVMSWs in a magnonic crystal by folding the dispersion for a uniform sample

$$\omega(k, H) = \sqrt{\omega_H \left(\omega_H + \omega_M \frac{1 - \exp(-kd)}{kd} \right)}, \quad (6)$$

where $\omega_H = \mu_0\gamma H$ and $\omega_M = \mu_0\gamma M$, into into the first Brillouin zone of the magnonic crystal [Fig. 2(a)], and then periodically translating it in the reciprocal space. Band gaps emerge at Brillouin-zone boundaries [Fig. 2(b)]. Yet, within the allowed bands, we can still approximate the effective force in a gradient magnetic field by applying Eq. (3) to Eq. (6), to obtain

$$F = -\frac{\mu_0\gamma G}{\omega_0} \left(\omega_H + \omega_M \frac{1 - \exp(-kd)}{2kd} \right), \quad (7)$$

which can be converted into a function of either just x or just k using Eqs. (1) and (6). This dependence of the force on x (and therefore k) has important consequences. Firstly, we expect the period of Bloch oscillations calculated from Eq. (4) to depend on the magnonic band. Secondly, the different spectral components within the wave packet will have slightly different values of T_B , causing its broadening over time. The same effects would also be observed if the gradient of the magnetic field G was coordinate dependent. Finally, the analytically complicated form of Eq. (7) makes it challenging to generate analytical results in a closed form. So, we proceed using numerical micromagnetic simulations instead.

Our simulations are performed using MUMAX software [44]. A $6\text{ mm} \times 1\text{ }\mu\text{m} \times 1\text{ }\mu\text{m}$ (length \times width \times thickness) stripe of a YIG-like material is discretized into $16384 \times 1 \times 1$ cuboidal cells with dimensions of $375\text{ nm} \times 1\text{ }\mu\text{m} \times 1\text{ }\mu\text{m}$, respectively [45]. To simulate an infinite magnonic crystal, two-dimensional (2D) periodic boundary conditions are used in the length and width directions. We assume the saturation magnetization of 200 kA/m , the exchange stiffness of 4 pJ/m^3 , and zero magnetocrystalline anisotropy. The assumed value of the Gilbert damping parameter is 0.0001 , as in high-quality YIG samples [46,47]. The sample is always magnetized along its length and therefore the direction of spin-wave propagation (BVMSW geometry), with equilibrium magnetization configuration established prior to dynamical simulations. Fourier transform techniques [39] are used to convert results of real space-time domain simulations into reciprocal space and/or frequency domain to recover the dispersion and other propagation characteristics of spin waves in our sample.

Figure 2(a) shows the magnonic dispersion relation calculated from the results of dynamic simulations with a broadband excitation (both in frequency domain and reciprocal space [39]) for a uniform bias magnetic field of 185 mT . Although the bias field and sample are both uniform, we use show the dispersion folded into the first Brillouin zone corresponding to the same sample but spatially modulated by an additional sinusoidal static magnetic field with a period of $3\text{ }\mu\text{m}$ (“empty lattice” approximation). The dispersion for the latter case is shown Fig. 2(b) for 10-mT amplitude of the field modulation. Both dispersions begin ($k = 0$) from the ferromagnetic resonance (FMR) frequency of about 8 GHz . The group velocity is negative, and so, the magnonic bands are ordered in frequency from top to bottom. The periodic sinusoidal modulation induces a large first band gap at frequency of about 7 GHz , while the other (higher-order) band gaps are significantly smaller, virtually negligible. Since the dispersion flattens at large k values [Fig. 2(a)], the higher-order magnonic bands also become increasingly flat [Fig. 2(b)].

To be observable, Bloch oscillations must have a period smaller than the BVMSW lifetime in YIG, which is typically on the order of hundreds of nanoseconds [46,47]. According to Eqs. (4) and (5), this favors greater lattice constants and field gradients. At the same time, the lattice constant must remain much smaller than the size L of the region within which the wave packet bounces back and forth (Fig. 1), so that we could justify our approximation of an adiabatically slow variation of the dispersion relation. To maintain the field gradient, the increase in size L required to accommodate a

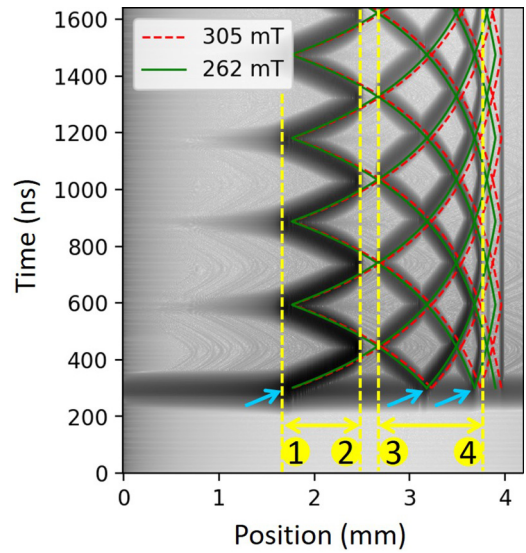


FIG. 3. The real space-time domain evolution of the BVMSW wave packets is shown for a field gradient of 40 mT/mm applied to a magnonic crystal with a lattice constant of $3\text{ }\mu\text{m}$. The grayscale shows the results of the numerical simulations (darker color corresponds to greater spin-wave amplitude), while the curves are the analytical wave-packet trajectories calculated using Eq. (9) for the field values of 262 and 305 mT . The vertical dashed lines and the double-headed arrows indicate boundaries and sizes, respectively, of the regions in which the wave packets are confined. The single-headed arrows indicate parts of the sample serving as spin-wave sources.

greater lattice constant needs to be matched by an increase of the bias magnetic field. However, the strength of the field (and therefore its gradients) achievable in the lab is limited. As a compromise, we have run our simulations for the field gradient G of 40 mT/mm , which should be feasible (albeit challenging) experimentally. The results of the simulations confirm that Bloch oscillations should be observable under such experimental conditions.

The grayscale in Fig. 3 shows the numerically simulated trajectories of spin-wave packets undergoing Bloch oscillations in our sample. To excite a BVMSW wave packet, we drive our sample by a burst of uniform microwave magnetic field with central frequency of 10 GHz , a Gaussian temporal envelope of 10-MHz bandwidth, and amplitude of 0.01 mT . The uniform microwave field couples to magnetic precession only where the local FMR frequency [48,49] is close to that of the microwave field, i.e., 10 GHz . In a process known as Schlömann mechanism of spin-wave emission [38,48,49], this part of the sample (shown as the leftmost single-headed arrow in Fig. 3) then serves as a source of propagating spin waves. The latter form a wave packet that propagates in the direction of increasing bias magnetic field, due to the negative dispersion of the BVMSWs. The wave packet is reflected from the large band gap, which separates the first magnonic band from the rest of the spectrum by a [Fig. 2(b)]. This leads to Bloch oscillations setting up in the first band, which hosts a single trajectory confined between lines 1 and 2 in Fig. 3.

The dispersion folding leads to spin-wave emission from a few additional, spatially separated regions, each emitting

wave packets in both directions (Fig. 3). As a result, each higher-order magnonic band is also populated with a wave packet. However, Landau-Zener tunneling through negligibly small band gaps leads to a complete transmission of the wave packets between adjacent bands [4,7,8,11,14,15]. This leads to a cyclic motion of multiple wave packets across multiple bands, i.e., all but the first one, evident from the multiple trajectories confined between lines 3 and 4 in Fig. 3. This represents an extreme case of Zener-Bloch oscillations [50], a phenomenon combining Bloch oscillations and Landau-Zener tunneling. The period of such Zener-Bloch oscillations is equal to the sum of Bloch periods for the bands traversed by the wave packet.

Let us have a closer look at the trajectories' shape. They can be calculated from the group velocity $v \equiv (\frac{\partial \omega}{\partial k})_H$ as

$$x(t) = \int v(t) dt = \int \frac{v}{F} dk, \quad (8)$$

where t is time and we have used Eq. (3). If, in addition, the force is constant, we obtain

$$x(t) = [\omega(k) - \omega(k_0)]/F \text{ and } k(t) = F(t - t_0) + k_0 \quad (9)$$

from Eqs. (8) and (3), respectively [51]. Equations (9) mean that the real space-time domain trajectory of a wave packet driven by a constant force must follow the dispersion curve. In our sample excited via the Schlömann mechanism, the BVMSW wave packet is excited at $t_0 \approx 300$ ns with $x_0 \approx 1.7$ mm for $\omega_0 = 2\pi \times 10$ GHz and $k_0 = 0$. Figure 3 shows the trajectories plotted using Eq. (9) with an assumption of a constant force $F = -\mu_0 \gamma G$ and with the field values of 262 and 305 mT used in Eq. (6), with the dispersion periodically “folded” into the first Brillouin zone (empty lattice approximation). The field of 262 mT corresponds to point x_0 at which the wave packet is excited in the first magnonic band. The field of 305 mT is the average over the entire sample, i.e., equal to the field at its center, $x = 3$ mm. Surprisingly, these approximate analytical trajectories reproduce the numerical data rather well. This is due to the width of the BVMSW band being weakly dependent on the field value. These observations are consistent with the linear dependence of the wave number on time that are observed in the simulations, as shown in Fig. 4.

In the frequency domain, the Bloch oscillations are observed as a system of discrete levels, which are separated by the Bloch frequency [11,13–15]. Indeed, the motion of the wave packet is cyclic and therefore confined. Positions of such confinement regions depend on the wave frequency and are therefore different for different levels. So, the levels are shifted in space along the field gradient, thereby forming what is known as a “Wannier ladder” (Fig. 5). To resolve the levels, the simulations are run over an increased duration and with a microwave excitation of bandwidth spanning the whole magnonic band spectrum. The levels are clearly detectable but the relatively small Bloch frequency of just about 3.45 MHz makes this task challenging.

In conclusion, we have used micromagnetic simulations to demonstrate Bloch oscillations and Wannier-ladder spectrum for magneto-dipole spin waves in the backward volume geometry under rather realistic experimental conditions.

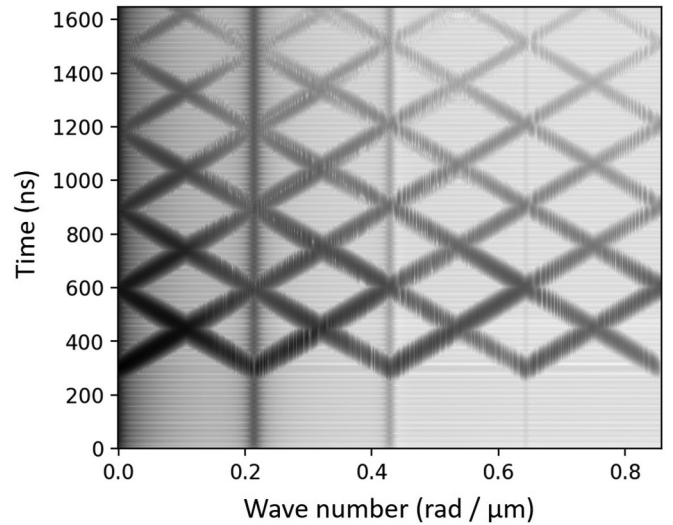


FIG. 4. The reciprocal space-time domain evolution of the BVMSW wave packets is shown for a field gradient of 40 mT/mm applied to a magnonic crystal with a lattice constant of 3 μm . The darker grayscale corresponds to greater Fourier amplitude of spin waves.

Scanning Brillouin light scattering microscopy and vector network analyzer-based spin-wave spectroscopy appear to be the best candidates to observe these phenomena in YIG-based systems experimentally. The requirement of a uniformly large gradient of the bias magnetic field appears to be the most

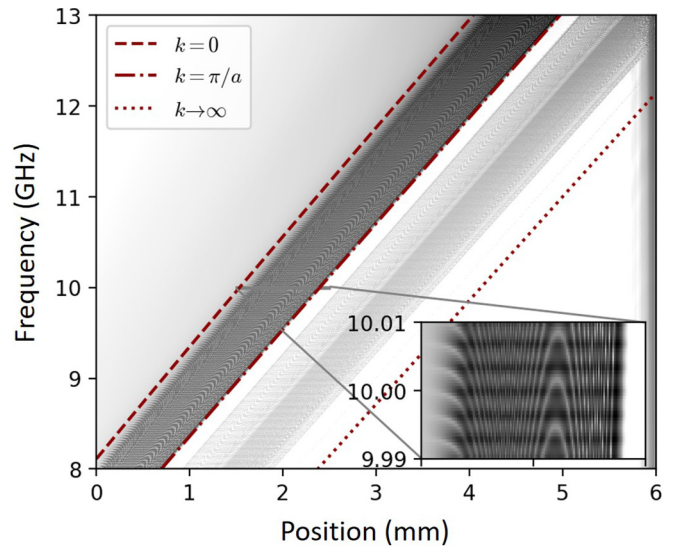


FIG. 5. The Wannier ladder is shown for a field gradient of 40 mT/mm applied to a magnonic crystal with a lattice constant of 3 μm . The grayscale shows the results of the numerical simulations (darker color corresponds to greater Fourier amplitude of spin waves), while the lines show the boundaries of the first magnonic band (short dashed and dashed-dotted) and the whole of the BVMSW band (short dashed and dotted), calculated using Eq. (6) for the characteristic values of the wave number, i.e., in the empty lattice approximation in the main panel. The inset is a zoomed image of the flat region indicated in the main panel.

stringent limitation. However, it could be overcome either through magnet engineering [52] or using alternative ways to create the required graded magnonic index [53]. These ideas could be extended to other magnonic geometries, systems, and concepts. Augmenting the graded magnonic index with a time dependence [54,55] appears a particularly interesting avenue for further research.

The research leading to these results has received funding from the Engineering and Physical Sciences Research Council of the United Kingdom, via the EPSRC Centre for Doctoral Training in Metamaterials (Grant No. EP/L015331/1), and from the European Union's Horizon 2020 research and innovation program under Marie Skłodowska-Curie Grant Agreement No. 644348 (MagIC).

-
- [1] F. Bloch, Über die Quantenmechanik der Elektronen in Kristallgittern, *Z. Phys.* **52**, 555 (1929).
- [2] K. Leo, P. H. Bolivar, F. Brüggemann, R. Schwedler, and K. Köhler, Observation of Bloch oscillations in a semiconductor superlattice, *Solid State Commun.* **84**, 943 (1992).
- [3] C. Waschke, H. G. Roskos, R. Schwedler, K. Leo, H. Kurz, and K. Köhler, Coherent Submillimeter-Wave Emission from Bloch Oscillations in a Semiconductor Superlattice, *Phys. Rev. Lett.* **70**, 3319 (1993).
- [4] C. Zener, A theory of the electrical breakdown of solid dielectrics, *Proc. R. Soc. A* **145**, 523 (1934).
- [5] R. Sapienza, P. Costantino, D. Wiersma, M. Ghulinyan, C. J. Oton, and L. Pavesi, Optical Analogue of Electronic Bloch Oscillations, *Phys. Rev. Lett.* **91**, 263902 (2003).
- [6] V. Agarwal, J. A. del Río, G. Malpuech, M. Zamfirescu, A. Kavokin, D. Coquillat, D. Scalbert, M. Vladimirova, and B. Gil, Photon Bloch Oscillations in Porous Silicon Optical Superlattices, *Phys. Rev. Lett.* **92**, 097401 (2004).
- [7] H. Trompeter, T. Pertsch, F. Lederer, D. Michaelis, U. Streppel, A. Bräuer, and U. Peschel, Visual Observation of Zener Tunneling, *Phys. Rev. Lett.* **96**, 023901 (2006).
- [8] H. Trompeter, W. Krolikowski, D. N. Neshev, A. S. Desyatnikov, A. A. Sukhorukov, Y. S. Kivshar, T. Pertsch, U. Peschel, and F. Lederer, Bloch Oscillations and Zener Tunneling in Two-Dimensional Photonic Lattices, *Phys. Rev. Lett.* **96**, 053903 (2006).
- [9] N. D. Lanzillotti Kimura, A. Fainstein, and B. Jusserand, Phonon Bloch oscillations in acoustic-cavity structures, *Phys. Rev. B* **71**, 041305(R) (2005).
- [10] N. D. Lanzillotti-Kimura, A. Fainstein, B. Perrin, B. Jusserand, O. Mauguin, L. Largeau, and A. Lemaître, Bloch Oscillations of THz Acoustic Phonons in Coupled Nanocavity Structures, *Phys. Rev. Lett.* **104**, 197402 (2010).
- [11] M. M. de Lima, Jr., Y. A. Kosevich, P. V. Santos, and A. Cantarero, Surface Acoustic Bloch Oscillations, the Wannier-Stark Ladder, and Landau-Zener Tunneling in a Solid, *Phys. Rev. Lett.* **104**, 165502 (2010).
- [12] M. Ben Dahan, E. Peik, J. Reichel, Y. Castin, and C. Salomon, Bloch Oscillations of Atoms in an Optical Potential, *Phys. Rev. Lett.* **76**, 4508 (1996).
- [13] S. R. Wilkinson, C. F. Bharucha, K. W. Madison, Q. Niu, and M. G. Raizen, Observation of Atomic Wannier-Stark Ladders in an Accelerating Optical Potential, *Phys. Rev. Lett.* **76**, 4512 (1996).
- [14] Q. Niu, X.-G. Zhao, G. A. Georgakis, and M. G. Raizen, Atomic Landau-Zener Tunneling and Wannier-Stark Ladders in Optical Potentials, *Phys. Rev. Lett.* **76**, 4504 (1996).
- [15] Y. Ke, X. Qin, H. Zhong, J. Huang, C. He, and C. Lee, Bloch-Landau-Zener dynamics in single-particle Wannier-Zeeman systems, *Phys. Rev. A* **91**, 053409 (2015).
- [16] Y. V. Kartashov, V. V. Konotop, D. A. Zezyulin, and L. Torner, Bloch Oscillations in Optical and Zeeman Lattices in the Presence of Spin-Orbit Coupling, *Phys. Rev. Lett.* **117**, 215301 (2016).
- [17] A. I. Akhiezer, V. G. Bar'yakhtar, and S. V. Peletminskii, *Spin Waves* (North-Holland, Amsterdam, 1968).
- [18] M. Krawczyk, J.-C. Lévy, D. Mercier, and H. Puzskarski, Forbidden frequency gaps in magnonic spectra of ferromagnetic layered composites, *Phys. Lett. A* **282**, 186 (2001).
- [19] S. A. Nikitov, P. Tailhades, and C. S. Tsai, Spin waves in periodic magnetic structures - magnonic crystals, *J. Magn. Mater.* **236**, 320 (2001).
- [20] S. Tacchi, G. Gubbiotti, M. Madami, and G. Carlotti, Brillouin light scattering studies of 2D magnonic crystals, *J. Phys.: Condens. Matter* **29**, 073001 (2017).
- [21] V. V. Kruglyak, S. O. Demokritov, and D. Grundler, Magnonics, *J. Phys. D: Appl. Phys.* **43**, 264001 (2010).
- [22] S. A. Nikitov, D. V. Kalyabin, I. V. Lisenkov, A. Slavin, Y. N. Barabanenkov, S. A. Osokin, A. V. Sadovnikov, E. N. Beginin, M. A. Morozova, Y. P. Sharaevsky *et al.*, Magnonics: A new research area in spintronics and spin wave electronics, *Phys. Usp.* **58**, 1002 (2015).
- [23] V. V. Kruglyak, C. S. Davies, V. S. Tkachenko, O. Y. Gorobets, Y. I. Gorobets, and A. N. Kuchko, Formation of the band spectrum of spin waves in 1D magnonic crystals with different types of interfacial boundary conditions, *J. Phys. D: Appl. Phys.* **50**, 094003 (2017), and references therein.
- [24] M. Krawczyk and D. Grundler, Review and prospects of magnonic crystals and devices with reprogrammable band structure, *J. Phys.: Condens. Matter* **26**, 123202 (2014), and references therein.
- [25] M. Pardavi-Horvath, Interaction effects in magnetic nanostructures, *Phys. Status Solidi A* **211**, 1030 (2014), and references therein.
- [26] A. A. Nikitin, A. B. Ustinov, A. A. Semenov, A. V. Chumak, A. A. Serga, V. I. Vasyuchka, E. Lahderanta, B. A. Kalinikos, and B. Hillebrands, A spin-wave logic gate based on a width-modulated dynamic magnonic crystal, *Appl. Phys. Lett.* **106**, 102405 (2015).
- [27] M. Krawczyk, S. Mamica, M. Mruczkiewicz, J. W. Klos, S. Tacchi, M. Madami, G. Gubbiotti, G. Duerr, and D. Grundler, Magnonic band structures in two-dimensional bi-component magnonic crystals with in-plane magnetization, *J. Phys. D: Appl. Phys.* **46**, 495003 (2013).
- [28] L. H. Bai, M. Kohda, and J. Nitta, Observation of spin wave modes depending on a tunable periodic magnetic field, *Appl. Phys. Lett.* **98**, 172508 (2011).
- [29] M. Vogel, A. V. Chumak, E. H. Waller, T. Langner, V. I. Vasyuchka, B. Hillebrands, and G. von Freymann, Optically reconfigurable magnetic materials, *Nat. Phys.* **11**, 487 (2015).

- [30] T. Langner, D. A. Bozhko, S. A. Bunyaev, G. N. Kakazei, A. V. Chumak, A. A. Serga, B. Hillebrands, and V. I. Vasyuchka, Spin-wave propagation through a magnonic crystal in a thermal gradient, *J. Phys. D: Appl. Phys.* **51**, 344002 (2018).
- [31] A. V. Vashkovskii and E. G. Lökk, Characteristics of a magnetostatic surface wave in a ferrite–dielectric structure embedded in a slowly varying nonuniform magnetic field, *J. Commun. Technol. Electron.* **46**, 1163 (2001).
- [32] K. R. Smith, M. J. Kabatek, P. Krivosik, and M. Wu, Spin wave propagation in spatially nonuniform magnetic fields, *J. Appl. Phys.* **104**, 043911 (2008).
- [33] V. E. Demidov, M. P. Kostylev, K. Rott, J. Munchenberger, G. Reiss, and S. O. Demokritov, Excitation of short-wavelength spin waves in magnonic waveguides, *Appl. Phys. Lett.* **99**, 082507 (2011).
- [34] N. Perez and L. Lopez-Diaz, Magnetic field induced spin-wave energy focusing, *Phys. Rev. B* **92**, 014408 (2015).
- [35] A. M. Kosevich, Bloch oscillations of magnetic solitons as an example of dynamical localization of quasiparticles in a uniform external field (Review), *Low Temp. Phys.* **27**, 513 (2001).
- [36] V. V. Gann and Y. A. Kosevich, Bloch oscillations of spin waves in a nonuniform magnetic field, *Low Temp. Phys.* **36**, 722 (2010).
- [37] G. Monsivais and C. L. Ordóñez-Romero, Band structure and Wannier-Stark ladders in the spin wave spectrum, *J. Magn. Magn. Mater.* **466**, 150 (2018).
- [38] E. Schlömann, Generation of spin waves in nonuniform magnetic field. I. Conversion of electromagnetic power into spin-wave power and vice versa, *J. Appl. Phys.* **35**, 159 (1964).
- [39] M. Dvornik, Y. Au, and V. V. Kruglyak, Micromagnetic simulations in magnonics, *Top. Appl. Phys.* **125**, 101 (2013).
- [40] The field should be treated as a general effective magnetic field, representing, e.g., exchange bias or modulated anisotropy as in Y. I. Gorobets, A. E. Zyubanov, A. N. Kuchko, and K. D. Shedzhuri, Spin-wave spectrum in magnets with a periodically modulated anisotropy, *Fiz. Tverd. Tela (St. Petersburg)* **34**, 1486 (1992).
- [41] This consideration is not actually limited to spin waves, while $H(x)$ could be any parameter controlling the dispersion of spin or other waves.
- [42] H. Sanchis-Alepuz, Y. A. Kosevich, and J. Sánchez-Dehesa, Acoustic Analogue of Electronic Bloch Oscillations and Resonant Zener Tunneling in Ultrasonic Superlattices, *Phys. Rev. Lett.* **98**, 134301 (2007).
- [43] Y. A. Kosevich and V. V. Gann, Magnon localization and Bloch oscillations in finite Heisenberg spin chains in an inhomogeneous magnetic field, *J. Phys.: Condens. Matter* **25**, 246002 (2013).
- [44] A. Vansteenkiste, J. Leliaert, M. Dvornik, M. Helsen, F. Garcia-Sanchez, and B. Van Waeyenberge, The design and verification of MuMax3, *AIP Adv.* **4**, 107133 (2014).
- [45] The use of cell size much greater than the exchange length is determined by the available computational power and is justified by the negligible effect of the exchange interaction on the magneto-dipole waves studied here.
- [46] H. Qin, G.-J. Both, S. J. Hämäläinen, L. Yao, and S. van Dijken, Low-loss YIG-based magnonic crystals with large tunable bandgaps, *Nat. Commun.* **9**, 5445 (2018).
- [47] Q. Wang, B. Heinz, R. Verba, M. Kewenig, P. Pirro, M. Schneider, T. Meyer, B. Lägél, C. Dubs, T. Brächer, and A. V. Chumak, Spin Pinning and Spin-Wave Dispersion in Nanoscopic Ferromagnetic Waveguides, *Phys. Rev. Lett.* **122**, 247202 (2019).
- [48] C. S. Davies, V. D. Poimanov, and V. V. Kruglyak, Mapping the magnonic landscape in patterned magnetic structures, *Phys. Rev. B* **96**, 094430 (2017).
- [49] F. B. Mushenok, R. Dost, C. S. Davies, D. A. Allwood, B. Inkson, G. Hrkac, and V. V. Kruglyak, Broadband conversion of microwaves into propagating spin waves in patterned magnetic structures, *Appl. Phys. Lett.* **111**, 042404 (2017).
- [50] B. M. Breid, D. Witthaut, and H. J. Korsch, Bloch-Zener oscillations, *New J. Phys.* **8**, 110 (2006).
- [51] W. Shockley, *Electrons and Holes in Semiconductors. With Application to Transistor Electronics* (Van Nostrand Company, Toronto, 1950), pp. 171–172.
- [52] V. N. Samofalov, D. P. Belozorov, and A. G. Ravlik, Strong stray fields in systems of giant magnetic anisotropy magnets, *Phys. Usp.* **56**, 269 (2013).
- [53] C. S. Davies and V. V. Kruglyak, Graded-index magnonics, *Low Temp. Phys.* **41**, 760 (2015).
- [54] A. V. Chumak, V. S. Tiberkevich, A. D. Karenowska, A. A. Serga, J. F. Gregg, A. N. Slavin, and B. Hillebrands, All-linear time reversal by a dynamic artificial crystal, *Nat. Commun.* **1**, 141 (2010).
- [55] S. Choi, J. Choi, R. Landig, G. Kucsko, H. Zhou, J. Isoya, F. Jelezko, S. Onoda, H. Sumiya, V. Khemani, C. von Keyserlingk, N. Y. Yao, E. Demler, and M. D. Lukin, Observation of discrete time-crystalline order in a disordered dipolar many-body system, *Nature (London)* **543**, 221 (2016).